

Multiple Similarity Drug-Target Interaction Prediction with Random Walks and Matrix Factorization

Bin Liu, Dimitrios Papadopoulos, Fragkiskos D. Malliaros, Grigorios Tsoumakas, *Member, IEEE*, Apostolos N. Papadopoulos

Abstract—The discovery of drug-target interactions (DTIs) is a very promising area of research with great potential. In general, the identification of reliable interactions among drugs and proteins can boost the development of effective pharmaceuticals. In this work, we leverage random walks and matrix factorization techniques towards DTI prediction. In particular, we take a multi-layered network perspective, where different layers correspond to different similarity metrics between drugs and targets. To fully take advantage of topology information captured in multiple views, we develop an optimization framework, called MDMF, for DTI prediction. The framework learns vector representations of drugs and targets that not only retain higher-order proximity across all hyper-layers and layer-specific local invariance, but also approximates the interactions with their inner product. Furthermore, we propose an ensemble method, called MDMF2A, which integrates two instantiations of the MDMF model that optimize surrogate losses of the area under the precision-recall curve (AUPR) and the area under the receiver operating characteristic curve (AUC), respectively. The empirical study on real-world DTI datasets shows that our method achieves significant improvement over current state-of-the-art approaches in four different settings. Moreover, the validation of highly ranked non-interacting pairs also demonstrates the potential of MDMF2A to discover novel DTIs.

Index Terms—Drug-target interaction prediction, random walks, matrix factorization, multiple similarity, multiplex heterogeneous network

1 INTRODUCTION

THE main objective of the drug discovery process is to identify drug-target interactions (DTIs) among numerous candidates. Although *in vitro* experimental testing can verify DTIs, it suffers from extremely high time and monetary costs. Computational (*in silico*) methods employ machine learning techniques [1], such as matrix factorization (MF) [2], kernel-based models [3], and deep learning [4], to efficiently infer a small amount of candidate drugs. This vastly shrinks the search scope and reduces the workload of experiment-based verification, thereby accelerating the drug discovery process significantly.

In the past, the chemical structure of drugs and the protein sequence of targets were the main source of information used for inferring candidate DTIs [5], [6]. Recently, with the advancements in clinical medical technology, abundant drug and target-related biological data from multifaceted sources are exploited to boost the accuracy of DTI prediction. Some methods utilize multiple types of drug and target similarities by integrating them into a single drug and target similarity [3], [7], [8], but in doing so discard the distinctive

information possessed by each similarity view.

In contrast, network-based approaches consider the diverse drug and target data as a (multiplex) heterogeneous DTI network that describes multiple aspects of drug and target relations—learning topology-preserving representations of drugs and targets to facilitate DTI prediction. Such models are often bridged with deep learning methodologies, including graph neural networks [4], [9], [10]. Nevertheless, although deep learning models achieve improved performance, they require larger amounts of training data, lack interpretability, and are computationally intensive.

A particular instance of network-based models are those based on *random walks* to compute graph embeddings [11]. However, these models typically perform embedding generation and interaction prediction as two independent tasks. Hence, their embeddings are learned in an unsupervised manner, failing to preserve the topology information from the interaction network [12], [13]. Random walk embedding methods are essentially factorizing a matrix capturing node co-occurrences within random walk sequences generated from the graph [14]—allowing to unify embedding generation and interaction prediction under a common MF framework. Nevertheless, the MF method proposed in [14] that approximates DeepWalk [15] can only handle single-layer networks. Thus, it is unable to fully exploit the topology information of multiple drug and target layers present in multiplex heterogeneous DTI networks.

To address the issues mentioned above, we propose the formulation of a DeepWalk-based MF model, called MDMF, which incorporates multiplex heterogeneous DTI network embedding generation and DTI prediction within a unified

• B. Liu, D. Papadopoulos, G. Tsoumakas, and A. N. Papadopoulos are with the School of Informatics, Aristotle University of Thessaloniki, 54124 Thessaloniki, Greece.

E-mail: {binliu, dpapadopo, greg, papadopo}@csd.auth.gr

• F. D. Malliaros is with Paris-Saclay University, CentraleSupélec, Inria, Centre for Visual Computing (CVN), 91190 Gif-Sur-Yvette, France
E-mail: fragkiskos.malliaros@centralesupelec.fr

This work has been submitted to the IEEE for possible publication. Copyright may be transferred without notice, after which this version may no longer be accessible.

Manuscript received XXX; revised XXX.

optimization framework. It learns vector representations of drugs and targets that not only capture the whole network topology via factorizing the hyper-layer DeepWalk matrix, but also preserve the layer-specific local invariance with the graph Laplacian for each drug and target similarity view. Based on this formulation, we instantiate two models that leverage surrogate losses to optimize two essential evaluation metrics in DTI prediction, namely the area under the precision-recall curve (AUPR) and the area under the receiver operating characteristic curve (AUC). In addition, we integrate the two models to consider the maximization of both metrics. Experimental results on DTI datasets under various prediction settings show that the proposed method outperforms state-of-the-art approaches, including deep learning models. Besides, the model can discover new DTIs, not reported in the dataset, which were later experimentally verified.

The rest of this article is organized as follows. In Section 2 important related work in the area is presented, whereas Section 3 introduces some fundamental concepts to keep the paper self-contained. The proposed approach is presented in detail in Section 4. Performance evaluation results are offered in Section 5 and finally, Section 6 concludes the work and presents future research directions.

2 RELATED WORK

In this section, we briefly present some representative relevant works in the field of DTI prediction. In the following three parts, we review the prediction models relying on traditional machine learning algorithms, graph representation learning methods, and deep learning models, respectively.

2.1 Traditional Machine Learning Approaches

Several conventional machine learning methods have been employed to infer potential DTIs by leveraging the drug and target information from a chemogenomic perspective. WkNNIR [5] utilizes the recovered interactions inferred from neighborhood information, i.e., interactions of drugs having similar chemical structures and targets possessing similar protein sequences, to predict new DTIs, and distinguishes the importance of drug and target views based on their local imbalance. NRLMF [6] trains a logistic matrix factorization model with neighborhood regularization on chemical and sequence based similarities, and assigns a higher weight to the minority interacting data. MSCMF [7], another matrix factorization method, learns two low-rank features that align to linear combinations of multiple drug and target similarities derived from diverse data sources, respectively. MLRE [16] learns low-rank representations for each drug and target similarity (view), and utilizes co-regularized spectral clustering to minimize the difference among these view-specific features. In [8], multiple similarities are linearly integrated with a weighting scheme that boosts the similarity with the higher local interaction consistency (LIC). In addition, three matrix factorization models incorporating the fused similarities are proposed to optimize AUPR and AUC, which are two metrics used to a great extent in the evaluation of DTI prediction. In DRLSM [3], multiple kernel learning based on the Hilbert–Schmidt Independence Criterion is employed to integrate multiple drug

and target similarities into two spaces (drug and target), upon which a dual Laplacian regularized least squares classifier is trained to make predictions. Furthermore, DTI prediction could be formulated as a classification task, which can be addressed by training binary [17] or multi-label classifiers [18] over the features derived from both drug and target sides.

A common disadvantage of traditional machine learning approaches, while trying to analyze the multi-layer similarity information, is the linear combination of the different similarity networks. Although the similarity fusion process in [3], [7], [8], [17] succeeds in unifying the heterogeneous information, it also heavily distorts the individual topology of each network layer, and subsequently hinders the model from extracting the unique insights offered by different similarity views. Another limitation for the broad majority of DTI prediction methods, including the subsequent graph embedding and deep learning models, is that they do not directly optimize the commonly used AUC and AUPR metrics.

2.2 Graph Embedding Approaches

Graph embedding approaches project the nodes of a graph on a low dimensional latent space in an unsupervised manner, while preserving the underlining topological structure of the graph. The intuition of random walk based approaches is that nodes appearing multiple times within the same random walks should belong to the same neighborhood and thus their vector representations should be similar to each other. In this part, representative random walk based embedding learning methods that support effective solutions for various downstream tasks are revisited, and their applications in DTI prediction are briefly reviewed.

Inspired by the advances in the field of natural language processing, DeepWalk [15] samples short random walks starting from each node of the graph to create node sequences, which are equivalent to word sequences in a document. Then, it employs the skip-gram language model to maximize the co-occurrence probability of nodes appearing in the same sequence. Node2Vec [19], as an improvement over DeepWalk, suggests a more sophisticated way to sample random walks, applying either a breadth-first search direction to explore network homophily or a depth-first search direction to explore structural symmetry. Both models have shown to implicitly perform factorization of a matrix that captures node co-occurrences within random walks [14]. This has further motivated to propose NetMF, a direct factorization model which significantly improves performance. More details about this model and its formulation are provided in Sec. 3.3.

All the above methods are designed for processing single-layer networks only. Although Multi2vec [20] considers multiplex networks, it generates different node embeddings for each layer and does not learn the embeddings for the whole network. Besides, the multiple types of proximity are not learned in a unified model, i.e., the embedding generation for first-order proximity is totally independent of the embedding generation for the second-order proximity. A detailed description of other graph representation learning techniques can be found in [11], [21].

Graph embedding methods are an important type of DTI prediction methods. DTINet [12] makes use of multiple heterogeneous data sources to generate drug and target embeddings by applying random walk with restart and diffusion component analysis. Then, it infers new interactions by projecting drug and target embeddings in the same space by measuring the geometric proximity. In NEDTP [13], drug and target embeddings are generated by a Node2Vec model with random walks sampled from diverse drug and target related sub-networks. Interaction prediction is accomplished by training a Gradient Boosting Decision Tree classifier using the binary dataset constructed upon the learned embeddings. The major limitation of most graph embedding approaches is that the interaction information is ignored in the embedding generation process.

2.3 Deep Learning Approaches

With deep neural networks showing consistently superior performance in the latest years in a plethora of different learning tasks, their adoption in the DTI prediction field is understandably rising [22].

NeoDTI [9] is a graph embedding method based on deep learning that leverages information from multiple heterogeneous sources and implements a graph convolution architecture. After extracting non-linear features from the heterogeneous graph, it applies a learning procedure that transforms the drug and target embeddings to preserve the topology of the networks. In [10] the authors propose GADTI, a graph autoencoder for DTI prediction. In the encoder, it uses a graph neural network (GNN) to aggregate first order node information, employing random walks with restart to gather higher order information. The decoder performs a bilinear transformation based on the DistMult model [23], that reconstructs the original network, from which the predicted edges with higher probability are considered as new interactions. DTIP [4] uses a feature-level attention mechanism to extract fine-grained information for drug, target, and disease nodes. It also conducts random walks with restart in the heterogeneous network to acquire node sequences, which are processed by a Bi-GRU based model with attention mechanism to generate the drug and target embeddings. At last, DTIP uses a multiple-layer convolutional neural network to produce the interaction predictions between the drug-target pairs. Apart from mining the DTI network, there are also some deep learning models generating high-level representations from raw chemical structures of drugs and amino acid sequences of targets [24], [25], [26].

Although deep learning methods can be powerful, they require a large number of data for training to generalize well and guarantee a superior predictive performance over traditional machine learning techniques. They also involve a very large number of parameters. Both of these factors contribute to a very high computational cost of the optimization process. In addition, GNNs, the state-of-the-art approaches for graph-based tasks, such as link prediction, are sensitive to noise [27], [28]. This is very important in the DTI prediction task since the bipartite network of drug-target interactions suffers from numerous yet undiscovered interactions [2], [5].

3 PRELIMINARIES

In this section, we present some fundamental concepts. More specifically, we introduce the problem formally and present briefly some key issues related to Matrix Factorization and Random Walks. Table 1 summarizes the most frequently used symbols.

TABLE 1
Frequently used symbols.

Symbol	Interpretation
D (T)	the set of training drugs (targets)
n_d (n_t)	number of training drugs (targets)
m_d (m_t)	number of drug (target) similarities or layers
$\mathbf{S}^{d,h}$ ($\mathbf{S}^{t,h}$)	the h -th (sparse) drug similarity matrix for D
$\mathbf{S}^{t,h}$ ($\mathbf{S}^{d,h}$)	the h -th (sparse) target similarity matrix for T
\mathbf{Y}	the interaction matrix between D and T
$\bar{\mathbf{s}}_x^{d,h}$	the similarity vector between test drug d_x and D
$\bar{\mathbf{s}}_z^{t,h}$	the similarity vector between test target t_z and T
\hat{Y}_{xz}	the prediction of the test pair (d_x, t_z)
r	the dimension of embeddings
\mathbf{U}	the learned embeddings of D
\mathbf{V}	the learned embeddings of T
$\mathbf{A}^{i,j}$	the adjacency matrix of a hyper-layer
$\mathbf{M}^{i,j}$	the DeepWalk matrix of hyper-layer $\mathbf{A}^{i,j}$
$\bar{\mathbf{M}}$	the DeepWalk matrix of the whole DTI network
w_i^d (w_j^t)	the LIC-based similarity weight for $\mathbf{S}^{d,i}$ ($\mathbf{S}^{t,j}$)

3.1 Problem Formulation

Given a drug set $D = \{d_i\}_{i=1}^{n_d}$ and a target set $T = \{t_i\}_{i=1}^{n_t}$, the relation between drugs (targets) can be assessed in various aspects, which are represented by a set of similarity matrices $\{\mathbf{S}^{d,h}\}_{h=1}^{m_d}$ ($\{\mathbf{S}^{t,h}\}_{h=1}^{m_t}$), where $\mathbf{S}^{d,h} \in \mathbb{R}^{n_d \times n_d}$ ($\mathbf{S}^{t,h} \in \mathbb{R}^{n_t \times n_t}$) and m_d (m_t) is the number of relation types for drugs (targets). In addition, let the binary matrix $\mathbf{Y} \in \{0, 1\}^{n_d \times n_t}$ indicate the interactions between drugs in D and targets in T , where $Y_{ij} = 1$ denotes that d_i and t_j interact with each other, and $Y_{ij} = 0$ otherwise. A DTI dataset for D and T consists of $\{\mathbf{S}^{d,h}\}_{h=1}^{m_d}$, $\{\mathbf{S}^{t,h}\}_{h=1}^{m_t}$ and \mathbf{Y} .

Let (d_x, t_z) be a test drug-target pair, $\{\bar{\mathbf{s}}_x^{d,h}\}_{h=1}^{m_d}$ be a set of n_d -dimensional vectors storing the similarities between d_x and D , and $\{\bar{\mathbf{s}}_z^{t,h}\}_{h=1}^{m_t}$ be a set of n_t -dimensional vectors storing the similarities between t_z and T . A DTI prediction model predicts a real-valued score \hat{Y}_{xz} indicating the confidence of the affinity between d_x and t_z . In addition, $d_x \notin D$ ($t_z \notin T$), which does not belong to the training set, is considered as the new drug (target). There are four prediction settings according to whether the drug and target involved in the test pair are training entities [29]:

- S1: predict the interaction between $d_x \in D$ and $t_z \in T$;
- S2: predict the interaction between $d_x \notin D$ and $t_z \in T$;
- S3: predict the interaction between $d_x \in D$ and $t_z \notin T$;
- S4: predict the interaction between $d_x \notin D$ and $t_z \notin T$.

3.2 Matrix Factorization for DTI Prediction

In DTI prediction, MF methods typically learn two vectorized representations of drugs and targets that approximate

the interaction matrix \mathbf{Y} by minimizing the following objective:

$$\min_{\mathbf{U}, \mathbf{V}} \mathcal{L}(\hat{\mathbf{Y}}, \mathbf{Y}) + \mathcal{R}(\mathbf{U}, \mathbf{V}), \quad (1)$$

where $\hat{\mathbf{Y}} = f(\mathbf{UV}^\top) \in \mathbb{R}^{n_d \times n_t}$ is the predicted interaction matrix, f is either the identity function ω for standard MF [2] or the element-wise logistic function σ for Logistic MF [6], and $\mathbf{U} \in \mathbb{R}^{n_d \times r}$, $\mathbf{V} \in \mathbb{R}^{n_t \times r}$ are r -dimensional drug and target latent features (embeddings), respectively. The objective in Eq. (1) includes two parts: $\mathcal{L}(\hat{\mathbf{Y}}, \mathbf{Y})$ is the loss function to evaluate the inconsistency between the predicted and ground truth interaction matrix, and $\mathcal{R}(\mathbf{U}, \mathbf{V})$ concerns the regularization of the learned embeddings.

Given a test drug-target pair (d_x, t_z) , its prediction with a specific instantiation of f is computed based on the embeddings of d_x ($\mathbf{U}_x \in \mathbb{R}^r$) and t_z ($\mathbf{V}_z \in \mathbb{R}^r$):

$$\hat{Y}_{xz} = \begin{cases} \mathbf{U}_x \mathbf{V}_z^\top, & \text{if } f = \omega \\ \left(1 + \exp(-\mathbf{U}_x \mathbf{V}_z^\top)\right)^{-1}, & \text{if } f = \sigma. \end{cases} \quad (2)$$

Considering that the drug (target) involved in the test pair could be a training entity from D (T) or a new arriving one, there are two ways to derive its embeddings accordingly. If d_x (t_z) is a training drug (target), its embeddings are directly extracted from \mathbf{U} (\mathbf{V}), e.g., \mathbf{U}_x is a row of \mathbf{U} corresponding to d_x . For a new drug (target), its feature vector is estimated by linearly aggregating the embeddings of its k -nearest training drugs (targets).

3.3 DeepWalk as Matrix Factorization

DeepWalk [15] is a widely used network representation learning approach, which generates a number of random walks over a graph to capture proximity among nodes. It then employs the skip-gram model to learn latent node embeddings by maximizing the likelihood of node co-occurrences within these random walk sequences. Qiu et al. [14] proved that the DeepWalk model could be interpreted as a matrix factorization task when the length of random walk approaches infinity. In particular, they introduced NetMF, a model that approximates DeepWalk to learn embeddings of a network G containing n nodes by factorizing the DeepWalk matrix defined as:

$$\mathbf{M} = \log \left(\max \left(1, \frac{\psi(\mathbf{A})}{n_s n_w} \left(\sum_{h=1}^{n_w} (\mathbf{\Lambda}^{-1} \mathbf{A})^h \right) \mathbf{\Lambda}^{-1} \right) \right), \quad (3)$$

where $\mathbf{A} \in \mathbb{R}^{n \times n}$ is the adjacency matrix of G , $\psi(\mathbf{A}) = \sum_i \sum_j A_{ij}$, $\mathbf{\Lambda} = \text{diag}(\mathbf{A}e)$ is a diagonal matrix with row sum of \mathbf{A} , n_w is the window size of the random walk controlling the number of context nodes, n_s plays the same role as the number of negative samples in DeepWalk, while the max function avoids having an invalid logarithm and guarantees that all elements in \mathbf{M} being non-negative. Considering the symmetry of \mathbf{M} for undirected networks, the factorization of the DeepWalk matrix could be expressed as $\mathbf{M} = \mathbf{Q}\mathbf{Q}^\top$, where $\mathbf{Q} \in \mathbb{R}^{n \times r}$ represents the r -dimensional network embeddings.

4 PROPOSED APPROACH

In this section, we first provide the general optimization framework of MDMF, which jointly learns topology preserving embeddings from a multiplex heterogeneous DTI network and reduces the inconsistency between predictions derived from these embeddings and ground-truth interactions. Then, we propose our models that follow the MDMF framework to minimize the AUPR and AUC losses and can infer DTIs for any new drug and target. The computational complexity of our method is analyzed at last.

4.1 Multiple Similarity DeepWalk-based Matrix Factorization (MDMF)

A DTI dataset, associated with multiple drug and target similarities, can be viewed as a multiplex heterogeneous network G^{DTI} . This can be done by treating drugs and targets as two types of vertices, and by considering non-zero similarities and interactions as edges connecting two homogeneous and heterogeneous entities respectively, where the weight of each edge equals the corresponding similarity or interaction value. Furthermore, in a DTI dataset, the similarity matrices are typically dense, as they are almost fully composed of non-zero elements, whereas the interaction matrix is a sparse one, including few non-zero values ("1"s). Consequently, similarity derived edges linking two drugs (targets) markedly outnumber bipartite edges representing the interactivity between drugs and targets in the DTI network, which inevitably reduces the influence of the more crucial interaction edges on the DTI prediction task. To balance the distribution of different types of edges and stress relations of more similar entities in the DTI network, we replace each original dense similarity matrix with the sparse adjacency matrix of its corresponding k -nearest neighbors (k -NNs) graph. Specifically, given a similarity matrix $\mathbf{S}^{d,h}$, its sparsified matrix $\hat{\mathbf{S}}^{d,h} \in \mathbb{R}^{n_d \times n_d}$ is defined as:

$$\hat{S}_{ij}^{d,h} = \begin{cases} S_{ij}^{d,h}, & \text{if } d_j \in \mathcal{N}_{d_i}^{k,h} \text{ and } d_i \in \mathcal{N}_{d_j}^{k,h} \\ 0, & \text{if } d_j \notin \mathcal{N}_{d_i}^{k,h} \text{ and } d_i \notin \mathcal{N}_{d_j}^{k,h} \\ \frac{1}{2} S_{ij}^{d,h}, & \text{otherwise,} \end{cases} \quad (4)$$

where $\mathcal{N}_{d_i}^{k,h}$ is the set of the k -NNs of d_i based on similarity $\mathbf{S}^{d,h}$.

Formally, G^{DTI} consists of three parts: (i) $G^d = \{\hat{\mathbf{S}}^{d,h}\}_{h=1}^{m_d}$, which is a multiplex drug subnetwork containing m_d layers, with $\hat{\mathbf{S}}^{d,h}$ being the adjacency matrix of the h -th drug layer; (ii) $G^t = \{\hat{\mathbf{S}}^{t,h}\}_{h=1}^{m_t}$, which is a multiplex target subnetwork including m_t layers with $\hat{\mathbf{S}}^{t,h}$ denoting the adjacency matrix of the h -th target layer; (iii) $G^Y = \mathbf{Y}$, which is a bipartite interaction subnetwork connecting drug and target nodes in each layer. Figure 1a depicts an example DTI network composed of three drug layers and two target layers. There are six identical bipartite interaction subnetworks, where each of them links nodes among a pair of drug and target layers.

The DeepWalk matrix cannot be directly calculated for the complex DTI network that includes two multiplex and a bipartite subnetwork. To facilitate its computation, we consider each combination of a drug and a target layer along

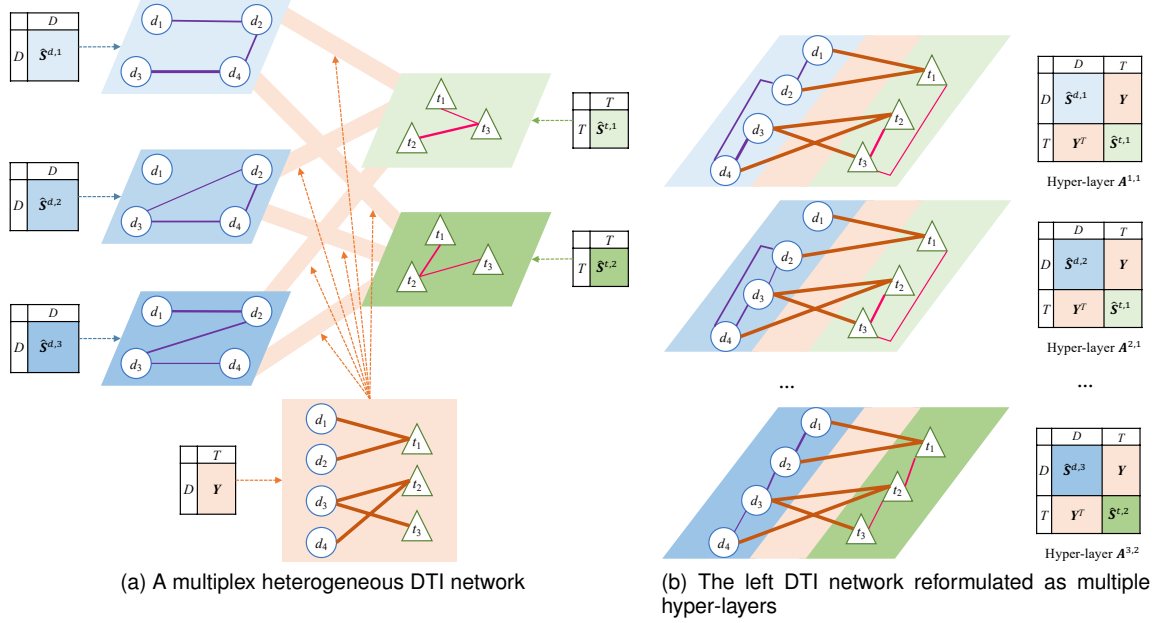


Fig. 1. Representing a DTI dataset with three drug and two target similarities as a network. (a) A multiplex heterogeneous network including three drug layers, two target layers, and six identical bipartite interaction subnetworks connecting drug and target nodes in each layer. (b) Six multiple hyper-layers, where each of them is composed of a drug and a target layer along with the interaction subnetwork.

with the interaction subnetwork as a hyper-layer, and reformulate the DTI network as a multiplex network containing $m_d \cdot m_t$ hyper-layers. The hyper-layer incorporating the i -th drug layer and j -th target layer, is defined by the adjacency matrix $A^{i,j} = \begin{bmatrix} \hat{S}^{d,i} & Y \\ Y^\top & \hat{S}^{t,j} \end{bmatrix}$, upon which G^{DTI} could be expressed as a set of hyper-layers $\{A^{i,j}\}_{i=1, j=1}^{m_d, m_t}$. Figure 1b illustrates the multiple hyper-layer network corresponding to the original DTI network in Figure 1a.

Based on the above reformulation, we compute a DeepWalk matrix $M^{i,j} \in \mathbb{R}^{(n_d+n_t) \times (n_d+n_t)}$ for each $A^{i,j}$ using Eq. (3), which reflects node co-occurrences in truncated random walks and captures richer proximity among nodes than the original hyper-layer—especially the proximity between unlinked nodes. In the example shown in Figure 2, d_4 and t_3 are two unlinked nodes in the original network, i.e., there is no bipartite edge connecting them ($A_{4,3}^{1,1} = 0$). On the other hand, $M_{4,3}^{1,1}$ is a non-zero value; this indicates that a certain level of proximity between d_4 and t_3 is found by the DeepWalk matrix, since there are random walk patches with length not exceeding four, such as $d_4 \rightarrow d_3 \rightarrow t_3$, traversing the two nodes. In addition, the relation between d_4 and t_3 represented by the DeepWalk matrix could also be interpreted as the recovery of their missing interaction, which supplements the incomplete interaction information and reduces the noise in the original dataset.

In order to mine multiple DeepWalk matrices effectively, we define a unified DeepWalk matrix for the whole DTI network by aggregating every $M^{i,j}$:

$$\bar{M} = \sum_{i=1}^{m_d} \sum_{j=1}^{m_t} w_i^d w_j^t M^{i,j}, \quad (5)$$

where w_i^d and w_j^t are weights of i -th drug and j -th target layers respectively with $\sum_{i=1}^{m_d} w_i^d = 1$ and $\sum_{j=1}^{m_t} w_j^t = 1$.

$A^{1,1}$	d_1	d_2	d_3	d_4	t_1	t_2	t_3
d_1	0	0.4	0	0	1	0	0
d_2	0.4	0	0	0.4	1	0	0
d_3	0	0	0	0.8	0	1	1
d_4	0	0.4	0.8	0	0	1	0
t_1	1	1	0	0	0	0	0.2
t_2	0	0	1	1	0	0	0.6
t_3	0	0	1	0	0.2	0.6	0

Fig. 2. Adjacency matrix $A^{1,1}$ of Figure 1b and its DeepWalk matrix $M^{1,1}$ with $n_w = 4$ and $n_s = 1$.

In Eq. (5), the importance of each hyper-layer is determined by multiplying the weights of its involved drug and target layers. In this work, we employ the LIC-based similarity weight, which assesses the proportion of proximate drugs (targets) having the same interactions, and has been found more effective than other similarity weights for DTI prediction [8].

Let $Q = \begin{bmatrix} U \\ V \end{bmatrix}$ be the vertical concatenation of drug and target embeddings. We encourage QQ^\top to approximate \bar{M} , which enables the learned embeddings to capture the topology information characterized by the holistic DeepWalk matrix. Hence, we derive the DeepWalk regularization term that diminishes the discrepancy between \bar{M} and QQ^\top :

$$\mathcal{R}_{dw}(U, V) = \|\bar{M} - QQ^\top\|_F^2. \quad (6)$$

Considering that the adjacency matrix $A^{i,j}$ includes four blocks, \bar{M} and QQ^\top could be divided into four blocks accordingly:

$$\bar{M} = \begin{bmatrix} \bar{M}_{S_d} & \bar{M}_Y \\ \bar{M}_Y^\top & \bar{M}_{S_t} \end{bmatrix} \quad QQ^\top = \begin{bmatrix} UU^\top & UV^\top \\ VU^\top & VV^\top \end{bmatrix}. \quad (7)$$

Thus, $\mathcal{R}_{dw}(U, V)$ can be expressed as the sum of norms of

these blocks as follows:

$$\mathcal{R}_{dw}(\mathbf{U}, \mathbf{V}) = \|\bar{\mathbf{M}}_{S_d} - \mathbf{U}\mathbf{U}^\top\|_F^2 + 2\|\bar{\mathbf{M}}_Y - \mathbf{U}\mathbf{V}^\top\|_F^2 + \|\bar{\mathbf{M}}_{S_t} - \mathbf{V}\mathbf{V}^\top\|_F^2. \quad (8)$$

However, aggregating all per-layer DeepWalk matrices to the holistic one inevitably leads to substantial loss of layer-specific topology information. To address this limitation, we employ graph regularization for each sparsified drug (target) layer to preserve per layer drug (target) proximity in the embedding space, i.e., similar drugs (targets) in each layer are likely to have similar latent features. To distinguish the utility of each layer, each graph regularization is multiplied by the LIC-based weight of its corresponding layer, which emphasizes the proximity of more reliable similarities. Furthermore, Tikhonov regularization is added to prevent latent features from overfitting the training set.

By replacing $\mathcal{R}(\mathbf{U}, \mathbf{V})$ in Eq. (1) with the above regularization terms, we arrive to the objective of MDMF:

$$\begin{aligned} \min_{\mathbf{U}, \mathbf{V}} \quad & \mathcal{L}(\hat{\mathbf{Y}}, \mathbf{Y}) + \frac{\lambda_M}{2} \mathcal{R}_{dw}(\mathbf{U}, \mathbf{V}) + \frac{\lambda_d}{2} \sum_{i=1}^{m_d} w_i^d \text{tr}(\mathbf{U}^\top \mathbf{L}_i^d \mathbf{U}) \\ & + \frac{\lambda_t}{2} \sum_{j=1}^{m_t} w_j^t \text{tr}(\mathbf{V}^\top \mathbf{L}_j^t \mathbf{V}) + \frac{\lambda_r}{2} (\|\mathbf{U}\|_F^2 + \|\mathbf{V}\|_F^2), \end{aligned} \quad (9)$$

where $\mathbf{L}_i^d = \text{diag}(\hat{\mathbf{S}}^{d,i} \mathbf{e}) - \hat{\mathbf{S}}^{d,i}$ and $\mathbf{L}_j^t = \text{diag}(\hat{\mathbf{S}}^{t,j} \mathbf{e}) - \hat{\mathbf{S}}^{t,j}$ are graph Laplacian matrices of $\hat{\mathbf{S}}^{d,i}$ and $\hat{\mathbf{S}}^{t,j}$ respectively, λ_M , λ_d , λ_t , and λ_r are regularization coefficients. In Eq. (9), the first term is a differentiable loss function which will be instantiated later, the second term is the proposed DeepWalk regularization capturing sufficient proximity from the whole network, the third and fourth terms concern the weighted sum of graph regularization for each layer, and the last term denotes the Tikhonov regularization.

Model optimization. The optimization problem of MDMF, shown in Eq. (9), can be solved by alternating optimization [2], [6]. In each iteration, \mathbf{U} is firstly updated with fixed \mathbf{V} , and then \mathbf{V} is updated with fixed \mathbf{U} . Let \mathcal{J} denote the objective function to be minimized in Eq. (9). Its gradients w.r.t. \mathbf{U} and \mathbf{V} are:

$$\begin{aligned} \nabla_{\mathbf{U}} \mathcal{J} = \nabla_{\mathbf{U}} \mathcal{L}(\hat{\mathbf{Y}}, \mathbf{Y}) + \lambda_d \sum_{i=1}^{m_d} w_i^d \mathbf{L}_i^d \mathbf{U} + \lambda_r \mathbf{U} + \\ 2\lambda_M ((\mathbf{U}\mathbf{U}^\top - \bar{\mathbf{M}}_{S_d})\mathbf{U} + (\mathbf{U}\mathbf{V}^\top - \bar{\mathbf{M}}_Y)\mathbf{V}) \end{aligned} \quad (10)$$

$$\begin{aligned} \nabla_{\mathbf{V}} \mathcal{J} = \nabla_{\mathbf{V}} \mathcal{L}(\hat{\mathbf{Y}}, \mathbf{Y}) + \lambda_t \sum_{j=1}^{m_t} w_j^t \mathbf{L}_j^t \mathbf{V} + \lambda_r \mathbf{V} + \\ 2\lambda_M ((\mathbf{V}\mathbf{V}^\top - \bar{\mathbf{M}}_{S_t})\mathbf{V} + (\mathbf{V}\mathbf{U}^\top - \bar{\mathbf{M}}_Y^\top)\mathbf{U}), \end{aligned} \quad (11)$$

where $\nabla_{\mathbf{U}} \mathcal{L}(\hat{\mathbf{Y}}, \mathbf{Y})$ and $\nabla_{\mathbf{V}} \mathcal{L}(\hat{\mathbf{Y}}, \mathbf{Y})$ are the gradients of the loss function for the two kinds of embeddings, respectively. The optimization algorithm of MDMF is illustrated in Algorithm 1, where θ is the learning rate. We firstly initialize \mathbf{U} and \mathbf{V} (Line 1), and calculate some auxiliary variables (Lines 2-6). Then, given an optimization method, which is either gradient descent (GD) or AdaGrad [30], we repeat the following procedure: changing \mathbf{U} based on $\nabla_{\mathbf{U}} \mathcal{J}$ and subsequently updating \mathbf{V} based on $\nabla_{\mathbf{V}} \mathcal{J}$, until convergence is achieved (Lines 9-22). In AdaGrad-based updating

Algorithm 1: Optimization Algorithm of MDMF

```

input :  $\mathbf{Y}, D, T, \{\mathbf{S}^{d,h}\}_{h=1}^{m_d}, \{\mathbf{S}^{t,h}\}_{h=1}^{m_t}, \theta, k,$ 
          $opti=GD$  or  $AdaGrad$ 
output:  $\mathbf{U}, \mathbf{V}$ 
1 Initialize  $\mathbf{U}$  and  $\mathbf{V}$  randomly;
2 for  $i \leftarrow 1$  to  $m_d$  do
3    $\lfloor$  Compute  $\hat{\mathbf{S}}^{d,i}, \mathbf{L}_i^d$  and  $w_i^d$ ;
4 for  $j \leftarrow 1$  to  $m_t$  do
5    $\lfloor$  Compute  $\hat{\mathbf{S}}^{t,j}, \mathbf{L}_j^t$  and  $w_j^t$ ;
6 Compute  $\bar{\mathbf{M}}$  according to Eq. (3) and Eq. (5);
7 if  $opti=AdaGrad$  then
8    $\mathbf{F}, \mathbf{H} \leftarrow \mathbf{0}, \mathbf{0}$ ; /* accumulated gradients
   used by AdaGrad */
9 repeat
10  Compute  $\nabla_{\mathbf{U}} \mathcal{J}$  according to Eq. (10);
11  if  $opti=AdaGrad$  then
12     $\mathbf{F} \leftarrow \mathbf{F} + (\nabla_{\mathbf{U}} \mathcal{J})^{\odot 2}$ ;
13     $\mathbf{U} \leftarrow \mathbf{U} - \theta \nabla_{\mathbf{U}} \mathcal{J} \odot \mathbf{F}^{\odot -\frac{1}{2}}$ ;
14  else
15     $\mathbf{U} \leftarrow \mathbf{U} - \theta \nabla_{\mathbf{U}} \mathcal{J}$ ;
16  Compute  $\nabla_{\mathbf{V}} \mathcal{J}$  according to Eq. (11);
17  if  $opti=AdaGrad$  then
18     $\mathbf{H} \leftarrow \mathbf{H} + (\nabla_{\mathbf{V}} \mathcal{J})^{\odot 2}$ ;
19     $\mathbf{V} \leftarrow \mathbf{V} - \theta \nabla_{\mathbf{V}} \mathcal{J} \odot \mathbf{H}^{\odot -\frac{1}{2}}$ ;
20  else
21     $\mathbf{V} \leftarrow \mathbf{V} - \theta \nabla_{\mathbf{V}} \mathcal{J}$ ;
22 until convergence;

```

steps (Lines 12-13 and 18-19), \odot is the Hadamard product operator, and $\odot a$ denotes the element wise exponentiation, with the exponent being a .

4.2 Optimizing Area Under the Curve with MDMF

4.2.1 Area Under the Curve Loss Functions

AUPR and AUC are two widely used area under the curve metrics in DTI prediction. Modeling differentiable surrogate losses that optimize these two metrics can lead to improvements in predicting performance [8]. Therefore, we instantiate the loss function in Eq. (9) with AUPR and AUC losses, and derive two DeepWalk-based MF models, namely MDMFAUPR and MDMFAUC, that optimize the AUPR and AUC metrics, respectively.

Given \mathbf{Y} and its predictions $\hat{\mathbf{Y}} = \sigma(\mathbf{U}\mathbf{V}^\top)$, which are sorted in descending order according to their predicted scores, AUPR without the interpolation to estimate the curve is computed as:

$$\text{AUPR}(\hat{\mathbf{Y}}, \mathbf{Y}) = \sum_{h=1}^{n_d n_t} \text{Prec}@h * \text{InRe}@h, \quad (12)$$

where $\text{Prec}@h$ is the precision of the h first predictions, $\text{InRe}@h$ is the incremental recall from rank $h-1$ to h . In addition, histogram binning [31], which assigns predictions into n_b ordered bins, is employed to simulate the non-differentiable and non-smooth sorting operation used to

rank predictions, deriving differential precision and incremental recall as:

$$\text{Prec}'@h = \frac{\sum_{i=1}^h \psi(\delta(\hat{\mathbf{Y}}, i) \odot \mathbf{Y})}{\sum_{i=1}^h \psi(\delta(\hat{\mathbf{Y}}, i))} \quad (13)$$

$$\text{InRe}'@h = \frac{1}{\psi(\mathbf{Y})} \psi(\delta(\hat{\mathbf{Y}}, h) \odot \mathbf{Y}), \quad (14)$$

where $\delta(\hat{\mathbf{Y}}, h)$ is the soft assignment function which returns the membership degree of each prediction to the h -th bin, i.e., $[\delta(\hat{\mathbf{Y}}, h)]_{ij} = \max(1 - |\hat{Y}_{ij} - b_h|/\Delta, 0)$, where b_h is the center of the h -th bin, and $\Delta = 1/(n_b - 1)$ is the bin width. Considering that maximizing AUPR is equivalent to minimizing $-\text{AUPR}(\hat{\mathbf{Y}}, \mathbf{Y})$, we obtain the differential AUPR loss according to Eq. (12)-(14):

$$\mathcal{L}_{AP} = - \sum_{h=1}^{n_b} \frac{\psi(\delta(\hat{\mathbf{Y}}, h) \odot \mathbf{Y}) \sum_{i=1}^h \psi(\delta(\hat{\mathbf{Y}}, i) \odot \mathbf{Y})}{\sum_{i=1}^h \psi(\delta(\hat{\mathbf{Y}}, i))}. \quad (15)$$

The objective of MDMFAUPR is given by using \mathcal{L}_{AP} to replace $\mathcal{L}(\hat{\mathbf{Y}}, \mathbf{Y})$ in Eq. (9).

In the optimization algorithm of MDMFAUPR, simple gradient descent is utilized for its computational efficiency, and the gradients of \mathcal{L}_{AP} w.r.t. \mathbf{U} and \mathbf{V} are:

$$\begin{aligned} \nabla_{\mathbf{U}} \mathcal{L}_{AP} &= \sum_{h=1}^{n_b} \frac{\psi_h}{(\tilde{\Psi}_h)^2} \left(\Psi_h \sum_{i=1}^h \tilde{\mathbf{Z}}^i \mathbf{V} - \tilde{\Psi}_h \sum_{i=1}^h \mathbf{Z}^i \mathbf{V} \right) \\ &\quad - \frac{\Psi_h}{\tilde{\Psi}_h} \mathbf{Z}^h \mathbf{V} \end{aligned} \quad (16)$$

$$\begin{aligned} \nabla_{\mathbf{V}} \mathcal{L}_{AP} &= \sum_{h=1}^{n_b} \frac{\psi_h}{(\tilde{\Psi}_h)^2} \left(\Psi_h \sum_{i=1}^h \tilde{\mathbf{Z}}^{i\top} \mathbf{U} - \tilde{\Psi}_h \sum_{i=1}^h \mathbf{Z}^{i\top} \mathbf{U} \right) \\ &\quad - \frac{\Psi_h}{\tilde{\Psi}_h} \mathbf{Z}^h \mathbf{U}, \end{aligned} \quad (17)$$

where $\tilde{\psi}_h = \psi(\delta(\hat{\mathbf{Y}}, h))$, $\psi_h = \psi(\delta(\hat{\mathbf{Y}}, h) \odot \mathbf{Y})$, $\Psi_h = \sum_{i=1}^h \psi_i$, $\tilde{\Psi}_h = \sum_{i=1}^h \tilde{\psi}_i$, $\tilde{\mathbf{Z}}^h = \nabla_{\hat{\mathbf{Y}}} \delta(\hat{\mathbf{Y}}, h) \odot \hat{\mathbf{Y}} \odot (\mathbf{1} - \hat{\mathbf{Y}})$, $\mathbf{Z}^h = \mathbf{Y} \odot \tilde{\mathbf{Z}}^h$.

AUC, which assesses the proportion of correctly ordered tuples, where the interacting drug-target pairs have higher prediction than the non-interacting ones, is defined as:

$$\text{AUC}(\hat{\mathbf{Y}}, \mathbf{Y}) = \frac{1}{|P|} \sum_{(ij, hl) \in P} \mathbb{I}[\hat{Y}_{ij} > \hat{Y}_{hl}], \quad (18)$$

where predictions $\hat{\mathbf{Y}} = \mathbf{U}\mathbf{V}^\top$ with $f = \omega$, and $P = \{(ij, hl) | (i, j) \in P_1, (h, l) \in P_0\}$ is the Cartesian product of $P_1 = \{(i, j) | Y_{ij} = 1\}$ and $P_0 = \{(i, j) | Y_{ij} = 0\}$. To maximize AUC, we need to minimize the proportion of wrongly ordered tuples, where the prediction of the interacting pair is lower than the non-interacting one. In order to make the AUC loss to be optimized easily, the discontinuous indicator function is substituted by a convex approximate function, i.e., $\phi(x) = \log(1 + \exp(-x))$, and the derived convex AUC loss is:

$$\mathcal{L}_{AUC} = \sum_{(ij, hl) \in P} \phi(\zeta_{ijhl}), \quad (19)$$

where $\zeta_{ijhl} = \hat{Y}_{ij} - \hat{Y}_{hl}$. With the substitution of $\mathcal{L}(\hat{\mathbf{Y}}, \mathbf{Y})$ with \mathcal{L}_{AUC} in Eq. (9), we obtain the objective of MDMFAUC.

Concerning the optimization of MDMFAUC, we employ the AdaGrad algorithm that adaptively changes the learning rate based on the accumulation of previous gradients to diminish the influence of sampling on computing gradients of \mathcal{L}_{AUC} . The gradients of \mathcal{L}_{AUC} w.r.t. \mathbf{U} and \mathbf{V} are:

$$\begin{aligned} \nabla_{\mathbf{U}} \mathcal{L}_{AUC} &= \left[(\nabla_{\mathbf{U}_1} \mathcal{L}_{AUC})^\top, \dots, (\nabla_{\mathbf{U}_{n_d}} \mathcal{L}_{AUC})^\top \right]^\top \\ \nabla_{\mathbf{U}_i} \mathcal{L}_{AUC} &\approx \sum_{(ij, hl) \in P'} \phi'(\zeta_{ijhl}) \mathbf{V}_j - \sum_{(hl, ij) \in P'} \phi'(\zeta_{hl ij}) \mathbf{V}_j \end{aligned} \quad (20)$$

$$\begin{aligned} \nabla_{\mathbf{V}} \mathcal{L}_{AUC} &= \left[(\nabla_{\mathbf{V}_1} \mathcal{L}_{AUC})^\top, \dots, (\nabla_{\mathbf{V}_{n_t}} \mathcal{L}_{AUC})^\top \right]^\top \\ \nabla_{\mathbf{V}_j} \mathcal{L}_{AUC} &\approx \sum_{(ij, hl) \in P'} \phi'(\zeta_{ijhl}) \mathbf{U}_i - \sum_{(hl, ij) \in P'} \phi'(\zeta_{hl ij}) \mathbf{U}_i, \end{aligned} \quad (21)$$

where P' is a $n_d n_t$ sized set sampled from P , which accelerates the computation of $\nabla_{\mathbf{U}} \mathcal{L}_{AUC}$ and $\nabla_{\mathbf{V}} \mathcal{L}_{AUC}$ to achieve linear complexity w.r.t. $n_d n_t$.

4.2.2 Inferring Embeddings of New Entities

When a new drug (target) arrives, MDMFAUPR and MDMFAUC infer its embeddings using its neighbors in the training set. As the new drug or target is associated with multiple similarities in the training data, we linearly integrate the different types of similarity with LIC-based weights to obtain the fused similarity vector:

$$\bar{\mathbf{s}}_x^\alpha = \sum_{h=1}^{m_\alpha} w_h^\alpha \bar{\mathbf{s}}_x^{\alpha, h}, \quad \alpha \in \{d, t\}, \quad (22)$$

where α_x is an unseen entity with $\alpha = d$ denoting a new drug and $\alpha = t$ indicating a novel target, and $\bar{\mathbf{s}}_x^\alpha \in \mathbb{R}^{n_\alpha}$ is the fused similarity vector of α_x . Based on $\bar{\mathbf{s}}_x^\alpha$, we retrieve the k -NNs of α_x from the training set, denoted as $\mathcal{N}_{\alpha_x}^k$, and estimate the embeddings of α_x as follows:

$$\begin{aligned} \mathbf{U}_x &= \frac{1}{\sum_{d_i \in \mathcal{N}_{d_x}^k} \bar{s}_{x i}^d} \sum_{d_i \in \mathcal{N}_{d_x}^k} \eta^{i'-1} \bar{s}_{x i}^d \mathbf{U}_i, \quad \text{if } \alpha = d \\ \mathbf{V}_x &= \frac{1}{\sum_{t_j \in \mathcal{N}_{t_x}^k} \bar{s}_{x j}^t} \sum_{t_j \in \mathcal{N}_{t_x}^k} \eta^{j'-1} \bar{s}_{x j}^t \mathbf{V}_j, \quad \text{if } \alpha = t, \end{aligned} \quad (23)$$

where $\bar{s}_{x i}^d$ is the similarity between d_x and d_i , i' (j') is the rank of d_i (t_j) among $\mathcal{N}_{d_x}^k$ ($\mathcal{N}_{t_x}^k$), e.g., $i' = 2$ if d_i is the second nearest training drug of d_x , and $\eta \in (0, 1]$ is the decay coefficient shrinking the weight of further neighbors, which is an important parameter to control the embedding aggregation. In addition, we employ a pseudo embedding based η selection strategy [8] to choose the optimal η values from a set of candidate \mathcal{C} for prediction settings involving new drugs or/and new targets, i.e., S2, S3, and S4, respectively. In MDMFAUPR, the η value leading to the best AUPR result is used, while the optimal η in MDMFAUC is the one achieving the best AUC result.

4.2.3 MDMF2A: Combining AUPR and AUC

It is known that both AUPR and AUC play a vital role in DTI prediction. However, MDMFAUPR and MDMFAUC only optimize one measure but ignore the other. To overcome this limitation, we propose an ensemble approach, called DWFM2A, which integrates the two MF models by

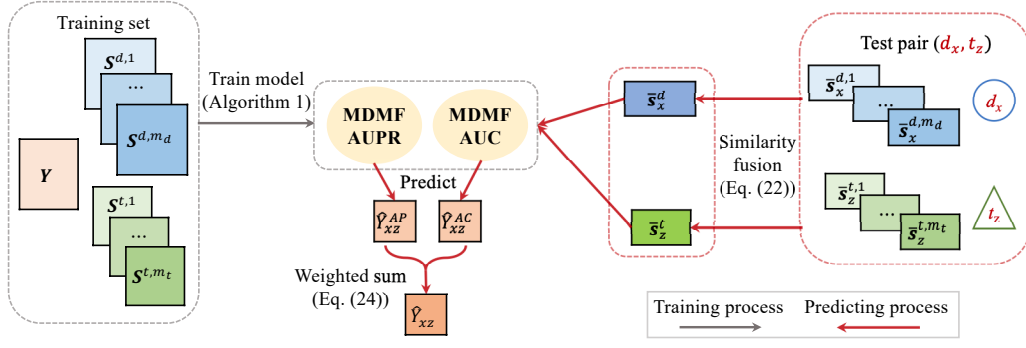


Fig. 3. The flowchart of MDMF2A. The DTI dataset is firstly used to train the two base models, namely MDMFAUPR and MDMFAUC, according to Algorithm 1. Then, given a test pair, if it involves any new drug or target, its associated similarity vectors are fused according to the LIC-based weights. Next, the two base models leverage these fused similarities to generate the estimation of the test pair, respectively. Lastly, MDMF2A aggregates the outputs of two models using Eq. (24) to obtain its final prediction.

aggregating their predicted scores. Given a test pair (d_x, t_z) , along with its predicted scores \hat{Y}_{xz}^{AP} and \hat{Y}_{xz}^{AC} obtained from MDMFAUPR and MDMFAUC respectively, the final prediction output by MDMF2A is defined as:

$$\hat{Y}_{xz} = \beta \hat{Y}_{xz}^{AP} + (1 - \beta) \sigma(\hat{Y}_{xz}^{AC}), \quad (24)$$

where $\beta \in [0, 1]$ is the trade-off coefficient for the two MF base models, and σ converts \hat{Y}_{xz}^{AC} and \hat{Y}_{xz}^{AP} into the same scale, i.e., $(0, 1)$. The flowchart of MDMF2A is shown in Figure 3.

4.3 Complexity Analysis

The complexity of MDMF is dominated by updating U and V , particularly, the computation of gradients in Eq. (10) and (11). In each iteration, the cost of obtaining $\nabla_U \mathcal{J}$ and $\nabla_V \mathcal{J}$ is $O(\nabla_U \mathcal{L}) + O(r(m_d n_d^2 + n_d n_t))$ and $O(\nabla_V \mathcal{L}) + O(r(m_t n_t^2 + n_d n_t))$ respectively, where $O(\nabla_U \mathcal{L})$ ($O(\nabla_V \mathcal{L})$) is the complexity of calculating the gradient of the loss function.

Considering $O(\nabla_U \mathcal{L}_{AP}) = O(\nabla_V \mathcal{L}_{AP}) = O(r n_b n_d n_t)$ for the AUPR loss, the overall computational cost of MDMFAUPR is $O(r n_b n_d n_t)$, as $n_b n_d n_t > m_d n_d^2$ and $n_b n_d n_t > m_d n_d^2$. The complexity of MDMFAUC, which utilizes \mathcal{L}_{AUC} with $O(\nabla_U \mathcal{L}_{AUC}) = O(\nabla_V \mathcal{L}_{AUC}) = O(r n_d n_t)$, is $O(r * \max\{m_d n_d^2, m_t n_t^2\})$. Lastly, MDMF2A, which integrates MDMFAUPR and MDMFAUC, requires a computational cost of $O(r(n_b n_d n_t + \max\{m_d n_d^2, m_t n_t^2\}))$.

5 PERFORMANCE EVALUATION

In this section, we present our results derived from the experimental study. Initially, we present the datasets that have been used and then describe the experimental setup and the associated results. Next, we present the ablation study and the impact of several parameters on the performance of the models. Finally, we show that our method is capable of discovering novel (previously unknown) DTIs.

5.1 Datasets

Two types of DTI datasets, constructed based on online biological and pharmaceutical databases, are used in this study. Their characteristics are shown in Table 2, where the

TABLE 2
Characteristics of datasets.

Dataset	n_d	n_t	$ P_1 $	Sparsity	m_d	m_t
NR	54	26	166	0.118		
GPCR	223	95	1096	0.052	4	4
IC	210	204	2331	0.054		
E	445	664	4256	0.014		
Luo	708	1512	1923	0.002	4	3

sparsity column equals $|P_1|/n_d n_t$, indicating the proportion of interacting pairs in the corresponding DTI dataset.

The first one is a collection of four golden standard datasets constructed by Yamanishi et al. [32] in 2007, each one corresponding to a target protein family, namely Nuclear Receptors (NR), Ion Channel (IC), G-protein coupled receptors (GPCR), and Enzyme (E). Because the interactions in these datasets were discovered 14 years ago, we have updated them by adding newly discovered interactions between drugs and targets in these datasets recorded in the last version of KEGG [33], DrugBank [34], and ChEMBL [35] databases. Four types of drug similarities, including SIMCOMP [36] built upon chemical structures, AERS-freq, AERS-bit [37] and SIDER [38] derived from drug side effects, as well as four types of target similarities, namely gene ontology (GO) term based semantic similarity, Normalized Smith–Waterman (SW), spectrum kernel with 3-mers length (SPEC-k3), and 4-mers length (SPEC-k4) based amino acid sequence similarities, obtained from [39] are utilized to describe diverse drug and target relations.

The second one provided by Luo et al. [12] (denoted as Luo), was built in 2017, includes DTIs and drug-drug interactions (DDI) obtained from DrugBank 3.0 [34], as well as drug side effect (SE) associations, protein–protein interactions (PPI) and disease-related associations extracted from SIDER [38], HPRD [40], and Comparative Toxicogenomics Database [41], respectively. Based on diverse drug and target interaction/association profiles, three drug similarities derived from DDI, SE and drug-disease associations as well as two target similarities derived from PPI and target-disease associations are computed. The Jaccard similarity coefficient is employed to assess the similarity of drugs, SEs or diseases (proteins or diseases) associated/interacted with two drugs

TABLE 3
AUPR results in all prediction settings.

Setting	Dataset	WkNNIR	MSCMF	NRMFL	MF2A	DRLSM	DTINet	NEDTP	NetMF	Multi2Vec	MDMF2A
S1	NR	-	0.628(5)	0.64(4)	0.673(2)	0.642(3)	0.508(7)	0.546(6)	0.455(8)	0.43(9)	0.675(1)
	GPCR	-	0.844(4)	0.86(3)	0.87(2)	0.835(5)	0.597(9)	0.798(7)	0.831(6)	0.747(8)	0.874(1)
	IC	-	0.936(3)	0.934(4)	0.943(2)	0.914(6)	0.693(9)	0.906(7)	0.929(5)	0.867(8)	0.946(1)
	E	-	0.818(5)	0.843(3)	0.858(2)	0.811(6)	0.305(9)	0.78(7)	0.831(4)	0.736(8)	0.859(1)
	Luo	-	0.599(5)	0.603(4)	0.653(2)	0.598(6)	0.216(8)	0.08(9)	0.615(3)	0.451(7)	0.679(1)
<i>AveRank</i>		-	4.4	3.6	2	5.2	8.4	7.2	5.2	8	1
S2	NR	0.562(4)	0.531(6)	0.547(5)	0.578(2)	0.57(3)	0.339(9)	0.486(7)	0.34(8)	0.338(10)	0.602(1)
	GPCR	0.54(3)	0.472(6)	0.508(5)	0.551(2)	0.532(4)	0.449(8)	0.451(7)	0.356(9)	0.254(10)	0.561(1)
	IC	0.491(3)	0.379(7.5)	0.479(4)	0.495(2)	0.466(5)	0.365(9)	0.407(6)	0.379(7.5)	0.16(10)	0.502(1)
	E	0.405(3)	0.288(7)	0.389(4)	0.422(2)	0.376(5)	0.173(9)	0.33(6)	0.269(8)	0.141(10)	0.428(1)
	Luo	0.485(2)	0.371(7)	0.458(5)	0.472(4)	0.502(1)	0.187(8)	0.077(10)	0.376(6)	0.079(9)	0.48(3)
<i>AveRank</i>		3	6.7	4.6	2.4	3.6	8.6	7.2	7.7	9.8	1.4
S3	NR	0.56(3)	0.505(6)	0.519(5)	0.588(1)	0.546(4)	0.431(7)	0.375(8)	0.359(9)	0.335(10)	0.582(2)
	GPCR	0.774(3)	0.69(6)	0.729(5)	0.787(2)	0.757(4)	0.546(9)	0.684(7)	0.638(8)	0.327(10)	0.788(1)
	IC	0.861(3)	0.827(6)	0.838(5)	0.863(2)	0.855(4)	0.599(9)	0.8(7)	0.791(8)	0.4(10)	0.865(1)
	E	0.728(3)	0.623(7)	0.711(5)	0.731(2)	0.712(4)	0.313(9)	0.615(8)	0.656(6)	0.257(10)	0.738(1)
	Luo	0.243(5)	0.08(7)	0.204(6)	0.292(3)	0.248(4)	0.061(8)	0.046(9)	0.294(2)	0.027(10)	0.299(1)
<i>AveRank</i>		3.4	6.4	5.2	2	4	8.4	7.8	6.6	10	1.2
S4	NR	0.309(1)	0.273(5)	0.278(4)	0.289(2)	0.236(7)	0.249(6)	0.16(8)	0.146(10)	0.149(9)	0.286(3)
	GPCR	0.393(3)	0.323(5)	0.331(4)	0.407(1.5)	0.077(9)	0.306(6)	0.29(7)	0.159(8)	0.074(10)	0.407(1.5)
	IC	0.339(3)	0.194(8)	0.327(4)	0.352(2)	0.086(9)	0.264(5)	0.251(6)	0.196(7)	0.067(10)	0.356(1)
	E	0.228(3)	0.074(8)	0.221(4)	0.235(2)	0.063(9)	0.1(6)	0.112(5)	0.09(7)	0.017(10)	0.239(1)
	Luo	0.132(3)	0.018(9)	0.096(5)	0.175(2)	0.061(6)	0.035(7)	0.03(8)	0.127(4)	0.002(10)	0.182(1)
<i>AveRank</i>		2.6	7	4.2	1.9	8	6	6.8	7.2	9.8	1.5
<i>Summary</i>		3*	6.13*	4.4*	2.08*	5.2*	7.85*	7.25*	6.68*	9.4*	1.28

(targets). In addition, drug similarity based on chemical structure and target similarity based on genome sequence are also computed. Therefore, four drug similarities and three target similarities are used for this dataset.

5.2 Experimental Setup

Following [29], four types of cross validation (CV) are conducted to examine the methods in four prediction settings, respectively. In S1, the 10-fold CV on pairs is used, where one fold of pairs is removed for testing. In S2 (S3), the 10-fold CV on drugs (targets) is applied, where one drug (target) fold along with its corresponding rows (columns) in Y is separated for testing. The 3×3 -fold block-wise CV, which splits a drug fold and target fold along with the interactions between them for testing, using the interactions between the remaining drugs and targets for training, is applied to S4. AUPR and AUC defined in Eq. (12) and (18) are used as evaluation measures.

To evaluate the performance of MDMF2A in all prediction settings, we have compared it to seven DTI prediction models (WkNNIR [5], NRLMF [6] MSCMF [7], MF2A [8], DRLSM [3], DTINet [12], NEDTP [13]) and two network embedding approaches applicable to any domain (NetMF [14] and Multi2Vec [20]). WkNNIR cannot perform predictions in S1, as it is specifically designed to predict interactions involving new drugs or/and targets (S2, S3, S4). In addition, the average of the corresponding multiple similarities are used as input for WkNNIR and NRLMF, since they can only handle a single type of drug and target similarity. NetMF, applicable to single-layer networks only, works on the holistic DeepWalk matrix \bar{M} that incorporates information from multiple hyper-layers. Multi2Vec, designed for multiplex networks, learns embeddings on the DTI network

composed of multiple hyper-layers, and averages the node vector representations across all hyper-layers as the final output embeddings. For both network embedding models, after the embedding learning process, we construct a binary training dataset, where each training drug-target pair (d_i, t_j) is transformed to an instance, whose feature vector is the concatenation of the embeddings of d_i and t_j and the label is Y_{ij} , and then employ it to train a random forest (RF) classifier with 100 trees using the Scikit-learn library [42]. A binary test dataset is built upon test pairs in a similar way, and the RF is used to predict the test set. Network embedding methods follow the transductive learning scheme, as test drugs (targets) should be available and utilized in the embedding learning process.

Furthermore, the proposed MDMF2A is compared to three deep learning-based methods, namely NeoDTI [9], GADTI [10], and DTIP [4]. These baselines can only be applied to the Luo dataset in S1, because they formulate the DTI dataset as a heterogeneous network consisting of four types of nodes (drugs, targets, drug-side effects, and diseases) and learn embeddings for all types of nodes.

The parameters of all baseline methods are set based on the suggestions in the respective articles. For MDMF2A, the trade-off ensemble weight β is chosen from $\{0, 0.01, \dots, 1.0\}$. For the two base models of MDMF2A, i.e., MDMFAUPR and MDMFAUC, the number of neighbors is set to $k = 5$, the window size of the random walk to $n_w = 5$, the number of negative samples to $n_s = 1$, the learning rate to $\theta = 0.1$, candidate decay coefficient set $C = \{0.1, 0.2, \dots, 1.0\}$, the embedding dimension r is chosen from $\{50, 100\}$, λ_d , λ_t and λ_r are chosen from $\{2^{-6}, 2^{-4}, 2^{-2}, 2^0, 2^2\}$, and $\lambda_M = 0.005$. The number of bins n_b in MDMFAUPR is chosen from $\{11, 16, 21, 26, 31\}$ for small and medium

TABLE 4
AUC results in all prediction settings.

Setting	Dataset	WkNNIR	MSCMF	NRMFL	MF2A	DRLSM	DTINet	NEDTP	NetMF	Multi2Vec	MDMF2A
S1	NR	-	0.882(3.5)	0.882(3.5)	0.884(2)	0.879(5)	0.797(8)	0.846(6)	0.818(7)	0.788(9)	0.892(1)
	GPCR	-	0.962(5)	0.972(3)	0.978(1.5)	0.971(4)	0.916(9)	0.953(7)	0.96(6)	0.93(8)	0.978(1.5)
	IC	-	0.982(5)	0.989(2)	0.989(2)	0.981(6.5)	0.938(9)	0.981(6.5)	0.985(4)	0.97(8)	0.989(2)
	E	-	0.961(7)	0.981(3)	0.983(2)	0.964(6)	0.839(9)	0.97(4)	0.966(5)	0.944(8)	0.984(1)
	Luo	-	0.922(6)	0.951(3)	0.966(2)	0.941(4)	0.894(8)	0.929(5)	0.917(7)	0.861(9)	0.97(1)
<i>AveRank</i>		-	5.3	2.9	1.9	5.1	8.6	5.7	5.8	8.4	1.3
S2	NR	0.825(5)	0.802(6)	0.826(4)	0.833(2)	0.831(3)	0.666(10)	0.786(7)	0.739(8)	0.727(9)	0.837(1)
	GPCR	0.914(3)	0.882(6)	0.913(4)	0.924(2)	0.867(7)	0.858(8)	0.885(5)	0.852(9)	0.811(10)	0.925(1)
	IC	0.826(3)	0.783(8)	0.825(4)	0.828(1)	0.796(6)	0.766(9)	0.794(7)	0.803(5)	0.715(10)	0.827(2)
	E	0.877(3)	0.835(6)	0.858(4)	0.892(2)	0.799(8)	0.78(9)	0.837(5)	0.811(7)	0.732(10)	0.895(1)
	Luo	0.904(5)	0.897(6)	0.917(3)	0.927(2)	0.864(8)	0.873(7)	0.907(4)	0.861(9)	0.776(10)	0.937(1)
<i>AveRank</i>		3.8	6.4	3.8	1.8	6.4	8.6	5.6	7.6	9.8	1.2
S3	NR	0.82(2)	0.786(6)	0.825(1)	0.819(3)	0.798(5)	0.756(7)	0.726(8)	0.712(9)	0.703(10)	0.805(4)
	GPCR	0.952(3)	0.902(8)	0.946(4)	0.96(2)	0.917(6)	0.879(9)	0.918(5)	0.909(7)	0.798(10)	0.961(1)
	IC	0.958(4)	0.941(6)	0.96(3)	0.967(1)	0.942(5)	0.907(9)	0.939(7)	0.938(8)	0.866(10)	0.966(2)
	E	0.935(4)	0.881(8)	0.936(3)	0.944(2)	0.883(7)	0.841(9)	0.918(5)	0.911(6)	0.815(10)	0.948(1)
	Luo	0.835(4)	0.826(8)	0.828(7)	0.901(2)	0.801(9)	0.829(6)	0.86(3)	0.831(5)	0.633(10)	0.902(1)
<i>AveRank</i>		3.4	7.2	3.6	2	6.4	8	5.6	7	10	1.8
S4	NR	0.637(4)	0.597(5)	0.656(2)	0.649(3)	0.592(6)	0.562(7)	0.548(8)	0.531(9)	0.524(10)	0.661(1)
	GPCR	0.871(3)	0.798(7)	0.866(4)	0.886(2)	0.405(10)	0.803(6)	0.816(5)	0.721(8)	0.581(9)	0.887(1)
	IC	0.774(4)	0.658(8)	0.775(3)	0.776(2)	0.498(10)	0.706(5)	0.702(6)	0.683(7)	0.555(9)	0.783(1)
	E	0.819(3)	0.695(7)	0.799(4)	0.821(2)	0.453(10)	0.757(5)	0.744(6)	0.69(8)	0.541(9)	0.827(1)
	Luo	0.819(4)	0.752(7)	0.804(5)	0.848(2)	0.438(10)	0.787(6)	0.822(3)	0.732(8)	0.513(9)	0.85(1)
<i>AveRank</i>		3.6	6.8	3.6	2.2	9.2	5.8	5.6	8	9.2	1
<i>Summary</i>		3.6*	6.43*	3.48*	1.98*	6.78*	7.75*	5.63*	7.1*	9.35*	1.33

datasets (NR, GPCR, and IC), while it is set to 21 for larger datasets (E and Luo). The source code of MDMF2A can be downloaded from https://github.com/intelligence-csd-auth-gr/DTI_MDMF2A.

5.3 Experimental Results

Tables 3 and 4 list the results of MDMF2A and its nine competitors on five datasets under four prediction settings. The numbers in the last row denote the average rank across all prediction settings, and “*” indicates that the advantage of DAMF2A over the competitor is statistically significant according to a Wilcoxon signed-rank test with Bergman-Hommel’s correction [43] at 5% level on the results of all prediction settings.

The proposed MDMF2A performs best in most cases for both metrics, achieving the highest average rank in all prediction settings and significantly outperforming all competitors. This demonstrates the effectiveness of our model to sufficiently exploit the topology information embedded in the multiplex heterogeneous DTI network and optimize the two area under the curve metrics. MF2A is the runner-up. Its inferiority to MDMF2A is mainly attributed to the ignorance of high-order proximity captured by random walks and the view-specific information loss caused by aggregating multi-type similarities. WkNNIR, NRMFL, DRLSM, and MSCMF come next. They are outperformed by the proposed MDMF2A, because they fail to capture the unique information provided by each view. The two graph embedding based DTI prediction models are usually inferior to other DTI prediction approaches, because they generate embedding in an unsupervised manner without exploiting the interacting information. Specifically, NEDTP using the class imbalance resilient GBDT as the predicting

classifier outperforms DTINet which employs simple linear projection to estimate DTIs. Regarding the two general multiplex network embedding methods, NetMF is better than Multi2Vec, because the latter requires dichotomizing the edge weights, which wipes out the different influence of the connected nodes in the similarity subnetwork. In addition, averaging all per-layer embeddings does not distinguish the importance of each hyper-layer, unlike the holistic DeepWalk Matrix used in NetMF, which contributes to the inferiority of Multi2Vec to NetMF as well.

There are some cases where MDMF2A does not achieve the best performance. Some competitors, such as WkNNIR, NRMFL and MF2A, are better than MDMF2A on NR datasets, implying that the random walk based embedding generation may not yield enough benefit in the case of small-sized datasets. Besides, concerning Luo dataset under S2, MDMF2A is outperformed by WkNNIR and DRLSM, which incorporate the neighborhood interaction recovery procedure, in terms of AUPR. In Luo dataset, the neighbor drugs are more likely to share the same interactions, leading to the effectiveness of neighborhood-based interaction estimation for new drugs. Nevertheless, the AUC results of the two competitors are 3.7% and 8.4% lower than DWFM2A, respectively. Also, MF2A is slightly better than MDMF2A on IC dataset in terms of AUC under S2 and S3, but the gap of results between them is tiny, e.g., 0.001.

The advantage of MDMF2A is also observed in the comparison with deep learning based DTI prediction models on Luo dataset. As shown in Table 5, MDMF2A outperforms all competitors in terms of AUPR, achieving 10% improvements over the best competitor (GADTI). In terms of AUC, MDMF2A is only 1.1% lower than DTIP, and 5.3% and 3.9% higher than NeoDTI and GADTI. Although DTIP

TABLE 5
Results of MDMF2A and deep learning models on Luo dataset in S1.

Metric	NeoDTI	GADTI	DTIP	MDMF2A
AUPR	0.573(3)	0.618(2)	0.399(4)	0.679(1)
AUC	0.921(4)	0.934(3)	0.981(1)	0.97(2)

slightly outperforms MDMF2A in terms of AUC, it suffers a significant decline in the AUPR result. Compared with deep learning competitors, MDMF2A takes full advantage of information shared by high-order neighbors and explicitly optimizes AUPR and AUC, resulting in better performance.

5.4 Ablation Study

To demonstrate the effectiveness of the ensemble framework and the regularization terms employed in the proposed method, we conduct an ablation study on MDMF2A by considering its five degenerate variants: (i) MDMFAUPR by setting β as 1; (ii) MDMFAUC by setting β as 0; (iii) MDMF2A-M excludes DeepWalk matrix based regularization, i.e., $\lambda_M = 0$; (iv) MDMF2A-dt does not consider layer-specific graph regularization i.e., $\lambda_d = \lambda_t = 0$; (v) MDMF2A-r ignores Tikhonov regularization, i.e., $\lambda_r = 0$. The average rank of MDMF2A and its five variants over all five datasets and four settings are shown in Figure 4. The detailed results are reported in Appendix Table A1.

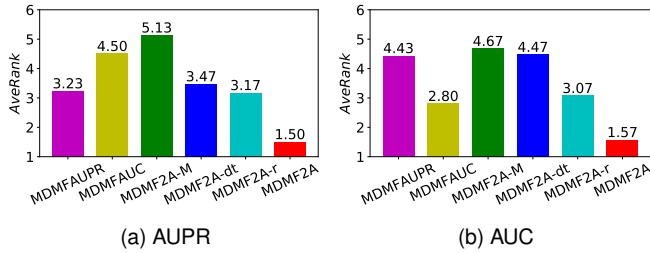


Fig. 4. The average rank of MDMF2A and its degenerate variants over all five datasets and four settings. Lower rank indicates better performance.

Firstly, although MDMFAUPR and MDMFAUC perform well in terms of the metric they optimize, they become worse in the other metric. MDMF2A outperforms its two base models in terms of both AUC and AUPR, verifying the success of integrating two single metric aware models in boosting performance. Concerning the regularization terms, we observe that removal of any term would trigger severe performance degradation, which confirms their importance in MDMF-based models. More specifically, DeepWalk matrix-based regularization, which captures high-order proximity from network topology, is the most crucial one. Layer-specific graph regularization that perverse distinctive information from each view comes next, and it contributes more to AUC. Although the damage caused by neglecting Tikhonov regularization is less than the other two, its function to avoid overfitting cannot be ignored.

5.5 Parameter Analysis

We further investigate the sensitivity of three important parameters: r , n_w and n_s . Figure 5 shows the AUC results of

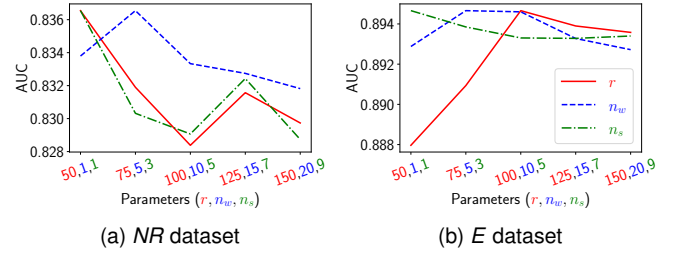


Fig. 5. AUC results of MDMF2A under different parameter configurations on NR and E dataset in S2.

MDMF2A under different parameter configurations on one smaller (NR) and one larger (E) dataset in S2. The influence of parameters in other prediction settings are presented in the Supplementary Appendix, Figures A1-A2.

Concerning the embedding dimension, r , lower values lead to better performance for the small-sized NR dataset. In the larger E dataset, the AUC result improves with higher values and plateaus when r reaches 100. For n_w , its optimal value is around 5 for both datasets. Smaller window size cannot exploit sufficient proximity among nodes, while a larger one incorporates unrelated nodes in the context, leading to performance deterioration. MDMF2A achieves the best performance when $n_s = 1$, and becomes worse when n_s increases, because a larger number of negative samples leads to a more sparse DeepWalk matrix, which cannot capture the structural information adequately. The impact of sparsity caused by larger n_s is more severe for the smaller NR dataset, whose corresponding DeepWalk matrix contains fewer non-zero values. Furthermore, the proposed model is more insensitive to DeepWalk related parameters, e.g., n_w and n_s , than the embedding dimension on E dataset. This demonstrates the robustness of MDMF2A to the parameter variation for mining large-scale networks.

5.6 Discovery of Novel DTIs

We examine the capability of MDMF2A to find novel DTIs not recorded in the Luo dataset. We do not consider updated golden standard datasets, since they have included all recently validated DTIs collected from up-to-date databases. We split all non-interacting pairs into 10 folds, and obtain predictions of each fold by training an MDMF2A model with all interacting pairs and the other nine folds of non-interacting ones. All non-interacting pairs are ranked based

TABLE 6
Top 10 new DTIs discovered by MDMF2A from Luo's datasets.

Drug ID	Drug name	Target ID	Target name	Rank	Database
DB00829	Diazepam	P48169	GABRA4	1	DB
DB01215	Estazolam	P48169	GABRA4	2	DB
DB00580	Valdecocix	P23219	PTGS1	3	-
DB01367	Rasagiline	P21397	MAOA	4	DC
DB00333	Methadone	P41145	OPRK1	5	DC
DB00363	Clozapine	P21918	DRD5	6	DC
DB06216	Asenapine	P21918	DRD5	7	DB
DB06800	Methylnaltrexone	P41143	OPRD1	8	DC
DB00802	Alfentanil	P41145	OPRK1	9	-
DB00482	Celecoxib	P23219	PTGS1	10	DC

on their predicting scores, and the top ten pairs are selected as newly discovered DTIs, which are shown in Table 6. To further verify the reliability of these new interaction candidates, we search their supportive evidence from DrugBank (DB) [34] and DrugCentral (DC) [44]. As we can see, 8/10 new interactions (in bold) are confirmed, demonstrating the success of MDMF2A in trustworthy new DTI discovery.

6 CONCLUSION AND FUTURE WORK

In this paper, we proposed MDMF2A, a random walk and matrix factorization based model to predict DTIs by effectively mining topology information from the multiplex heterogeneous network involving diverse drug and target similarities. It integrates two base predictors that leverage our designed objective function, encouraging the learned embeddings to preserve holistic network and layer-specific topology structures. The two base models utilize the convex AUPR and AUC losses in their objectives, enabling MDMF2A to simultaneously optimize two crucial metrics in the DTI prediction task. We conducted extensive experiments on five DTI datasets under various prediction settings. The results affirmed the superiority of the proposed MDMF2A to other competing DTI prediction methods. Furthermore, the practical ability of MDMF2A to discover novel DTIs was supported by the evidence from online biological databases.

In the future, we plan to extend our model to handle attributed DTI networks, including both topological and feature information for drugs and targets.

ACKNOWLEDGMENTS

B. Liu is supported from the China Scholarship Council (CSC) under the Grant CSC No.201708500095. F. D. Malliaros is supported in part by ANR under the JCJC project GraphIA (ANR-20-CE23-0009-01).

REFERENCES

- [1] M. Bagherian, E. Sabeti, K. Wang, M. A. Sartor, Z. Nikolovska-Coleska, and K. Najarian, "Machine learning approaches and databases for prediction of drug-target interaction: A survey paper," *Brief. Bioinformatics*, vol. 22, no. 1, pp. 247–269, 2021.
- [2] A. Ezzat, P. Zhao, M. Wu, X. L. Li, and C. K. Kwok, "Drug-target interaction prediction with graph regularized matrix factorization," *IEEE/ACM Trans. Comput. Biol. Bioinform.*, vol. 14, no. 3, pp. 646–656, 2017.
- [3] Y. Ding, J. Tang, and F. Guo, "Identification of drug-target interactions via dual laplacian regularized least squares with multiple kernel fusion," *Knowl. Based. Syst.*, vol. 204, p. 106254, 2020.
- [4] P. Xuan, Y. Zhang, H. Cui, T. Zhang, M. Guo, and T. Nakaguchi, "Integrating multi-scale neighbouring topologies and cross-modal similarities for drug-protein interaction prediction," *Brief. Bioinformatics*, vol. 22, no. 5, p. bbab119, 2021.
- [5] B. Liu, K. Pliakos, C. Vens, and G. Tsoumakas, "Drug-target interaction prediction via an ensemble of weighted nearest neighbors with interaction recovery," *Applied Intelligence*, 2021.
- [6] Y. Liu, M. Wu, C. Miao, P. Zhao, and X. L. Li, "Neighborhood regularized logistic matrix factorization for drug-target interaction prediction," *PLoS Comput. Biol.*, vol. 12, no. 2, p. e1004760, 2016.
- [7] X. Zheng, H. Ding, H. Mamitsuka, and S. Zhu, "Collaborative matrix factorization with multiple similarities for predicting drug-Target interactions," in *Proc. ACM SIGKDD Int. Conf. Knowl. Discov. Data Min.*, 2013, pp. 1025–1033.
- [8] B. Liu and G. Tsoumakas, "Optimizing area under the curve measures via matrix factorization for drug-target interaction prediction," *arXiv*, 2021.
- [9] F. Wan, L. Hong, A. Xiao, T. Jiang, and J. Zeng, "NeoDTI: Neural integration of neighbor information from a heterogeneous network for discovering new drug-target interactions," *Bioinformatics*, vol. 35, no. 1, pp. 104–111, 2019.
- [10] Z. Liu, Q. Chen, W. Lan, H. Pan, X. Hao, and S. Pan, "GADTI: graph autoencoder approach for DTI prediction from heterogeneous network," *Frontiers in Genetics*, vol. 12, 2021.
- [11] Z. Huang, A. Silva, and A. Singh, "A Broader Picture of Random-walk Based Graph Embedding," in *Proc. ACM SIGKDD Int. Conf. Knowl. Discov. Data Min.*, 2021, pp. 685–695.
- [12] Y. Luo, X. Zhao, J. Zhou, J. Yang, Y. Zhang, W. Kuang, J. Peng, L. Chen, and J. Zeng, "A network integration approach for drug-target interaction prediction and computational drug repositioning from heterogeneous information," *Nat. Commun.*, vol. 8, no. 1, pp. 1–13, 2017.
- [13] Q. An and L. Yu, "A heterogeneous network embedding framework for predicting similarity-based drug-target interactions," *Brief. Bioinformatics*, vol. 22, no. 6, pp. 1–10, 2021.
- [14] J. Qiu, Y. Dong, H. Ma, J. Li, K. Wang, and J. Tang, "Network embedding as matrix factorization: Unifying deepwalk, line, pte, and node2vec," in *Proc. ACM Int. Conf. Web Search Data Min.*, 2018, pp. 459–467.
- [15] B. Perozzi, R. Al-Rfou, and S. Skiena, "DeepWalk: Online learning of social representations," in *Proc. ACM SIGKDD Int. Conf. Knowl. Discov. Data Min.*, 2014, pp. 701–710.
- [16] L. Li and M. Cai, "Drug target prediction by multi-view low rank embedding," *IEEE/ACM Trans. Comput. Biol. Bioinform.*, vol. 16, no. 5, pp. 1712–1721, 2019.
- [17] R. S. Olayan, H. Ashoor, and V. B. Bajic, "DDR: Efficient computational method to predict drug-Target interactions using graph mining and machine learning approaches," *Bioinformatics*, vol. 7, no. 34, pp. 1164–1173, 2018.
- [18] K. Pliakos, C. Vens, and G. Tsoumakas, "Predicting drug-target interactions with multi-label classification and label partitioning," *IEEE/ACM Trans. Comput. Biol. Bioinform.*, vol. 18, no. 4, pp. 1596–1607, 2021.
- [19] A. Grover and J. Leskovec, "node2vec: Scalable feature learning for networks," in *Proc. ACM SIGKDD Int. Conf. Knowl. Discov. Data Min.*, 2016, pp. 855–864.
- [20] X. Teng, J. Liu, and L. Li, "A synchronous feature learning method for multiplex network embedding," *Information Sciences*, vol. 574, pp. 176–191, 2021.
- [21] B. Li and D. Pi, "Network representation learning: a systematic literature review," *Neural. Comput. Appl.*, vol. 32, no. 21, pp. 16 647–16 679, Nov. 2020.
- [22] M. Sun, S. Zhao, C. Gilvary, O. Elemento, J. Zhou, and F. Wang, "Graph convolutional networks for computational drug development and discovery," *Brief. Bioinformatics*, vol. 21, no. 3, pp. 919–935, 2020.
- [23] B. Yang, W. t. Yih, X. He, J. Gao, and L. Deng, "Embedding entities and relations for learning and inference in knowledge bases," in *International Conference on Learning Representations*, 2015.
- [24] K. Y. Gao, A. Fokoue, H. Luo, A. Iyengar, S. Dey, and P. Zhang, "Interpretable drug target prediction using deep neural representation," in *International Joint Conference on Artificial Intelligence (IJCAI)*, 2018, pp. 3371–3377.
- [25] Z. Cheng, C. Yan, F. Wu, and J. Wang, "Drug-target interaction prediction using multi-head self-attention and graph attention network," *IEEE/ACM Trans. Comput. Biol. Bioinform.*, 2021.
- [26] Z. Yu, J. Lu, Y. Jin, and Y. Yang, "KenDTI: an ensemble model based on network integration and CNN for drug-target interaction prediction," *IEEE/ACM Trans. Comput. Biol. Bioinform.*, vol. 18, no. 4, pp. 1305–1314, 2021.
- [27] H. Dai, H. Li, T. Tian, X. Huang, L. Wang, J. Zhu, and L. Song, "Adversarial attack on graph structured data," in *International Conference on Machine Learning (ICML)*, 2018, pp. 1115–1124.
- [28] D. Zügner, A. Akbarnejad, and S. Günnemann, "Adversarial attacks on neural networks for graph data," in *Proc. ACM SIGKDD Int. Conf. Knowl. Discov. Data Min.*, 2018, pp. 2847–2856.
- [29] T. Pahikkala, A. Airola, S. Pietilä, S. Shakyawar, A. Szwarda, J. Tang, and T. Aittokallio, "Toward more realistic drug-target interaction predictions," *Brief. Bioinformatics*, vol. 16, no. 2, pp. 325–337, 2015.
- [30] J. Duchi, E. Hazan, and Y. Singer, "Adaptive subgradient methods for online learning and stochastic optimization," *J. Mach. Learn. Res.*, vol. 12, pp. 2121–2159, 2011.

- [31] J. Revaud, J. Almazan, R. Rezende, and C. D. Souza, "Learning with average precision: Training image retrieval with a listwise loss," in *Proc. IEEE Int. Conf. Comput. Vis.*, 2019, pp. 5106–5115.
- [32] Y. Yamanishi, M. Araki, A. Gutteridge, W. Honda, and M. Kanehisa, "Prediction of drug-target interaction networks from the integration of chemical and genomic spaces," *Bioinformatics*, vol. 24, no. 13, p. i232–i240, 2008.
- [33] M. Kanehisa, M. Furumichi, M. Tanabe, Y. Sato, and K. Morishima, "KEGG: New perspectives on genomes, pathways, diseases and drugs," *Nucleic Acids Res.*, vol. 45, no. D1, pp. D353–D361, 2017.
- [34] D. S. Wishart, Y. D. Feunang, A. C. Guo, E. J. Lo, A. Marcu, J. R. Grant, T. Sajed, D. Johnson, C. Li, Z. Sayeeda, N. Assempour, I. Iynkkaran, Y. Liu, A. Maclejewski, N. Gale, A. Wilson, L. Chin, R. Cummings, D. Le, A. Pon, C. Knox, and M. Wilson, "DrugBank 5.0: A major update to the DrugBank database for 2018," *Nucleic Acids Res.*, vol. 46, no. D1, pp. D1074–D1082, 2018.
- [35] D. Mendez, A. Gaulton, A. P. Bento, J. Chambers, M. De Veij, E. Félix, M. P. Magariños, J. F. Mosquera, P. Mutowo, M. Nowotka, M. Gordillo-Marañón, F. Hunter, L. Junco, G. Mugumbate, M. Rodriguez-Lopez, F. Atkinson, N. Bosc, C. J. Radoux, A. Segura-Cabrera, A. Hersey, and A. R. Leach, "ChEMBL: Towards direct deposition of bioassay data," *Nucleic Acids Res.*, vol. 47, no. D1, pp. D930–D940, 2019.
- [36] M. Hattori, Y. Okuno, S. Goto, and M. Kanehisa, "Development of a chemical structure comparison method for integrated analysis of chemical and genomic information in the metabolic pathways," *J. Am. Chem. Soc.*, vol. 125, no. 39, pp. 11 853–11 865, 2003.
- [37] M. Takarabe, M. Kotera, Y. Nishimura, S. Goto, and Y. Yamanishi, "Drug target prediction using adverse event report systems: a pharmacogenomic approach," *Bioinformatics*, vol. 28, no. 18, p. i611–i618, 2012.
- [38] M. Kuhn, I. Letunic, L. J. Jensen, and P. Bork, "The SIDER database of drugs and side effects," *Nucleic Acids Research*, vol. 44, no. D1, pp. D1075–D1079, 2016.
- [39] A. C. Nascimento, R. B. Prudêncio, and I. G. Costa, "A multiple kernel learning algorithm for drug-target interaction prediction," *BMC Bioinformatics*, vol. 17, no. 1, pp. 1–16, 2016.
- [40] T. S. Keshava Prasad, R. Goel, K. Kandasamy, S. Keerthikumar, S. Kumar, S. Mathivanan, D. Telikicherla, R. Raju, B. Shafreen, A. Venugopal, L. Balakrishnan, A. Marimuthu, S. Banerjee, D. S. Somanathan, A. Sebastian, S. Rani, S. Ray, C. J. Harrys Kishore, S. Kanth, M. Ahmed, M. K. Kashyap, R. Mohmood, Y. I. Ramachandra, V. Krishna, B. A. Rahiman, S. Mohan, P. Ranganathan, S. Ramabadran, R. Chaerkady, and A. Pandey, "Human protein reference database-2009 update," *Nucleic Acids Res.*, vol. 37, no. suppl_1, p. D767–D772, 2009.
- [41] A. P. Davis, C. G. Murphy, R. Johnson, J. M. Lay, K. Lennon-Hopkins, C. Saraceni-Richards, D. Sciaky, B. L. King, M. C. Rosenstein, T. C. Wiegiers, and C. J. Mattingly, "The comparative toxicogenomics database: Update 2013," *Nucleic Acids Res.*, vol. 41, no. D1, pp. D1104–D1114, 2013.
- [42] F. Pedregosa, G. Varoquaux, A. Gramfort, V. Michel, B. Thirion, O. Grisel, M. Blondel, P. Prettenhofer, R. Weiss, V. Dubourg, J. Vanderplas, A. Passos, D. Cournapeau, M. Brucher, M. Perrot, and E. Duchesnay, "Scikit-learn: Machine learning in Python," *J. Mach. Learn. Res.*, vol. 12, pp. 2825–2830, 2011.
- [43] A. Benavoli, G. Corani, and F. Mangili, "Should we Really Use Post-Hoc Tests Based on Mean-Ranks?" *J. Mach. Learn. Res.*, vol. 17, no. 1, pp. 1–10, 2016.
- [44] S. Avram, C. G. Bologa, J. Holmes, G. Bocci, T. B. Wilson, D. T. Nguyen, R. Curpan, L. Halip, A. Bora, J. J. Yang, J. Knockel, S. Sirimulla, O. Ursu, and T. I. Oprea, "DrugCentral 2021 supports drug discovery and repositioning," *Nucleic Acids Res.*, vol. 49, no. D1, pp. D1160–D1169, 2021.

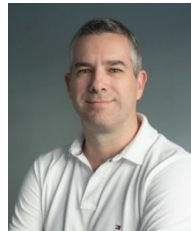
Bin Liu received an M.S. degree in computer science from Chongqing University of Posts and Telecommunications, China in 2016. He received a Ph.D degree in computer science from Aristotle University of Thessaloniki, Greece in 2022. His research interests include multi-label learning, class imbalance and bioinformatics.



Dimitrios Papadopoulos received a diploma in Information & Communication Systems Engineering from the University of Aegean in 2019, and an M.S. in Data Science from the Aristotle University of Thessaloniki (AUTH) in 2021. He is currently pursuing a Ph.D. degree in Machine Learning from AUTH. His research interests include supervised machine learning, graph mining, and drug discovery.



Fragkiskos D. Malliaros is an assistant professor at Paris-Saclay University, CentraleSupélec and associate researcher at Inria Saclay. He also co-directs the M.Sc. Program in Data Sciences and Business Analytics (CentraleSupélec and ESSEC Business School). Right before that, he was a postdoctoral researcher at UC San Diego (2016–17) and at École Polytechnique (2015–16). He received his Ph.D. in Computer Science from École Polytechnique (2015) and his M.Sc. degree from the University of Patras, Greece (2011). He is the recipient of the 2012 Google European Doctoral Fellowship in Graph Mining, the 2015 Thesis Prize by École Polytechnique, and best paper awards at TextGraphs-NAACL 2018 and ICWSM 2020 (honorable mention). In the past, he has been the co-chair of various data science-related workshops, and has also presented twelve invited tutorials at international conferences in the area of graph mining. His research interests span the broad area of data science, with focus on graph mining, machine learning, and network analysis.



Grigorios Tsoumakas received a degree in Informatics from the Aristotle University of Thessaloniki (AUTH) in 1999, an MSc in Artificial Intelligence from the University of Edinburgh in 2000 and a PhD in Informatics from AUTH in 2005. He is an Associate Professor of Machine Learning and Knowledge Discovery at the School of Informatics of AUTH since 2020, where he has also served as Assistant Professor (2013 – 2020) and Lecturer (2007 – 2013). His research expertise focuses on supervised machine learning (ensemble methods, multi-target prediction) and document intelligence (semantic indexing, keyphrase extraction, summarization). He has published more than 100 articles and according to Google Scholar his work has received more than 14,000 citations and his h-index is 44. Dr. Tsoumakas is a member of the IEEE and a senior member of the ACM.



Apostolos N. Papadopoulos is Associate Professor of Computer Science at the School of Informatics of Aristotle University of Thessaloniki (AUTH). He received his 5-year Diploma Degree in Computer Engineering and Informatics from the University of Patras, and his Ph.D. Degree in Informatics from the School of Informatics (AUTH). His research interests include Data Management, Data Mining and Big Data Analytics. He has co-presented four tutorials in ASONAM 2015, EDBT/ICDT 2016, ICDM 2016 and ECML/PKDD 2017 on the "Core Decomposition of Networks". The paper "SkyGraph: an algorithm for important subgraph discovery in relational graphs", Proceedings of ECML/PKDD, Antwerp, Belgium, 2008, received the Best Knowledge Discovery Paper Award, whereas the paper "Metric-Based Top-*k* Dominating Queries", Proceedings of the 17th International Conference on Extending Database Technology (EDBT), Athens, 2014, was selected as the best paper for publication in ACM Transactions on Database Systems. Based on Google Scholar, he has around 3700 citations in his research work.

Multiple Similarity Drug-Target Interaction Prediction with Random Walks and Matrix Factorization Appendix

Bin Liu¹, Dimitrios Papadopoulos¹, Fragkiskos D. Malliaros², Grigorios Tsoumakas,
*Member, IEEE*¹, and Apostolos N. Papadopoulos¹

¹School of Informatics, Aristotle University of Thessaloniki, 54124 Thessaloniki,
Greece.

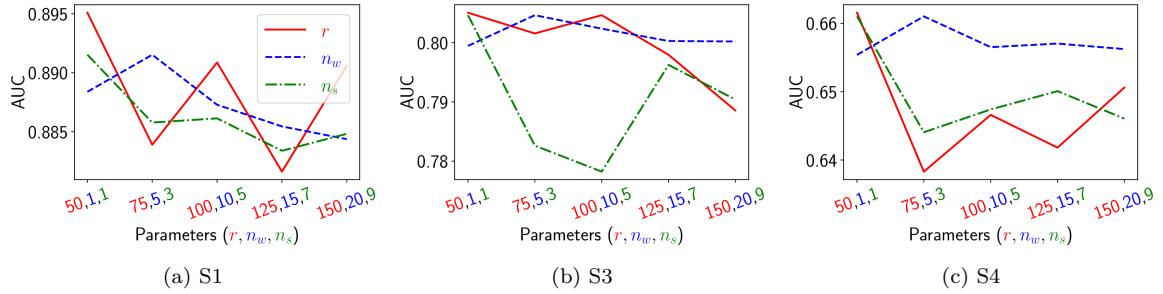
²Paris-Saclay University, CentraleSupélec, Inria, Centre for Visual Computing (CVN),
91190 Gif-Sur-Yvette, France

Appendix Table A1: Detailed AUPR results of ablation study.

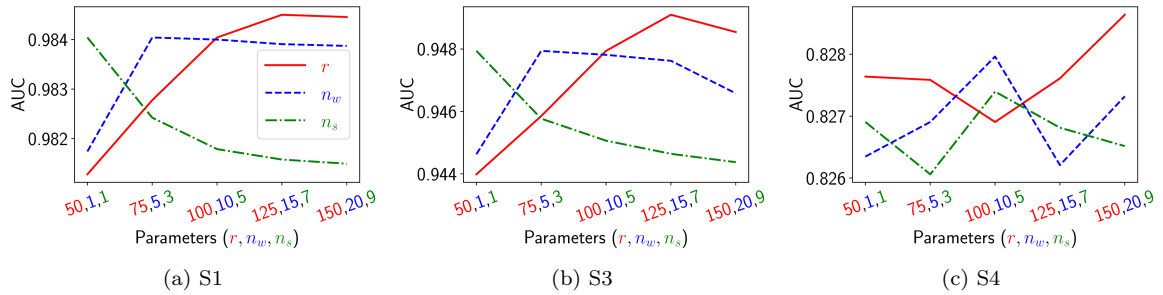
Setting	Dataset	MDMFAUPR	MDMFAUC	MDMF2A-M	MDMF2A-dt	MDMF2A-r	MDMF2A
S1	NR	0.671	0.657	0.641	0.557	0.671	0.675
	GPCR	0.867	0.874	0.867	0.77	0.875	0.874
	IC	0.943	0.929	0.943	0.92	0.942	0.946
	E	0.846	0.846	0.851	0.81	0.859	0.859
	Luo	0.677	0.6	0.641	0.641	0.681	0.679
S2	NR	0.595	0.547	0.571	0.592	0.594	0.602
	GPCR	0.558	0.539	0.515	0.546	0.562	0.561
	IC	0.495	0.492	0.47	0.499	0.501	0.502
	E	0.417	0.411	0.393	0.424	0.421	0.428
	Luo	0.472	0.448	0.355	0.466	0.474	0.48
S3	NR	0.582	0.545	0.536	0.545	0.543	0.582
	GPCR	0.785	0.779	0.746	0.762	0.768	0.788
	IC	0.861	0.863	0.853	0.865	0.843	0.865
	E	0.722	0.729	0.704	0.728	0.725	0.738
	Luo	0.278	0.265	0.455	0.277	0.292	0.299
S4	NR	0.284	0.277	0.26	0.269	0.274	0.286
	GPCR	0.406	0.402	0.354	0.399	0.407	0.407
	IC	0.353	0.343	0.345	0.358	0.346	0.356
	E	0.236	0.222	0.217	0.247	0.238	0.239
	Luo	0.18	0.157	0.189	0.172	0.183	0.182
<i>AveRank</i>		3.23	4.5	5.13	3.47	3.17	1.5

Appendix Table A2: Detailed AUC results of ablation study.

Setting	Dataset	MDMFAUPR	MDMFAUC	MDMF2A-M	MDMF2A-dt	MDMF2A-r	MDMF2A
S1	NR	0.888	0.885	0.873	0.836	0.887	0.892
	GPCR	0.977	0.977	0.977	0.97	0.978	0.978
	IC	0.988	0.988	0.988	0.984	0.989	0.989
	E	0.983	0.983	0.977	0.974	0.984	0.984
	Luo	0.968	0.968	0.952	0.959	0.969	0.97
S2	NR	0.832	0.83	0.82	0.83	0.831	0.837
	GPCR	0.917	0.925	0.913	0.911	0.924	0.925
	IC	0.819	0.826	0.806	0.814	0.826	0.827
	E	0.876	0.894	0.893	0.885	0.887	0.895
	Luo	0.935	0.929	0.903	0.927	0.935	0.937
S3	NR	0.803	0.821	0.787	0.788	0.807	0.805
	GPCR	0.957	0.963	0.961	0.961	0.959	0.961
	IC	0.963	0.966	0.964	0.966	0.966	0.966
	E	0.941	0.946	0.929	0.94	0.946	0.948
	Luo	0.888	0.895	0.898	0.882	0.9	0.902
S4	NR	0.66	0.649	0.671	0.661	0.66	0.661
	GPCR	0.878	0.887	0.884	0.882	0.886	0.887
	IC	0.781	0.779	0.759	0.781	0.777	0.783
	E	0.807	0.826	0.819	0.811	0.823	0.827
	Luo	0.846	0.849	0.813	0.838	0.85	0.85
<i>AveRank</i>		4.43	2.8	4.67	4.47	3.07	1.57



Appendix Figure A1: AUC results of MDMF2A under different parameter configurations on the NR dataset in S1, S3, and S4.



Appendix Figure A2: AUC results of MDMF2A under different parameter configurations on the E dataset in S1, S3, and S4.